*metals*

*Article*

# Enhancement of the Electrical Conductivity and Mechanical Properties of Al-Mg-Si and Al-Mg-Zn Ternary Systems After a T8 Heat Treatment

**Xóchitl Atanacio-Sánchez [1], Carlos Gamaliel Garay-Reyes [1], Alfredo Martínez-García [1], Ivanovich Estrada-Guel [1,*], José Manuel Mendoza-Duarte [1], Pedro Guerrero-Seañez [1], Sergio González-Sánchez [2], Enrique Rocha-Rangel [3], José de Jesús Cruz-Rivera [4], Emmanuel José Gutiérrez-Castañeda [4,5] and Roberto Martínez-Sánchez [1,4,*]**

[1] Centro de Investigación en Materiales Avanzados, Avenida Miguel de Cervantes Saavedra 120, Chihuahua 31136, Chihuahua, Mexico; xochitl.atanacio@cimav.edu.mx (X.A.-S.); carlos.garay@cimav.edu.mx (C.G.G.-R.); alfredo.martinez@cimav.edu.mx (A.M.-G.); jose.mendoza@cimav.edu.mx (J.M.M.-D.); pedro.guerrero@cimav.edu.mx (P.G.-S.)
[2] Faculty of Engineering and Environment, Northumbria University, Newcastle upon Tyne NE1 8ST, UK; sergio.sanchez@northumbria.ac.uk
[3] Research Department, Universidad Politécnica de Victoria, Av. Nuevas Tecnologías 5902, Parque Científico y Tecnológico de Tamaulipas, Cd. Victoria 87138, Tamaulipas, Mexico; erochar@upv.edu.mx
[4] Instituto de Metalurgia, Universidad Autónoma de San Luis Potosí, Sierra Leona No. 550, San Luis Potosí 78210, San Luis Potosí, Mexico; jdjcr35@uaslp.mx (J.d.J.C.-R.); emmanuel.gutierrez@uaslp.mx (E.J.G.-C.)
[5] CONAHCYT-UASLP, Universidad Autónoma de San Luis Potosí, Sierra Leona No. 550, San Luis Potosí 78210, San Luis Potosí, Mexico
* Correspondence: ivanovich.estrada@cimav.edu.mx (I.E.-G.); roberto.martinez@cimav.edu.mx (R.M.-S.); Tel.: +52-614-439-4813 (I.E.-G.); +52-614-439-1146 (R.M.-S.)

**Abstract:** The present research focuses on enhancing the mechanical properties and the electrical conductivity of alloys corresponding to the Al-Mg-Zn (two different compositions) and Al-Mg-Si systems, compared with the commercial 6201-T8 and 1350-H16 alloys, by using a novel approach based on T8 tempering (solution heat treated, cold worked, then artificially aged). After T8 tempering, the Al-Mg-Zn and Al-Mg-Si alloy systems show a better combination of electrical and mechanical properties, with an enhancement of the electrical conductivity by about 2.8% compared to that of 1350 alloy and 13% higher than for the 6201 alloy series. All studied alloys exhibit better mechanical properties than 1350-H16 and are similar to those of 6201-T8.

**Keywords:** Al-Mg-Zn system; Al-Mg-Si system; mechanical properties; electrical conductivity; thermal treatments



**Citation:** Atanacio-Sánchez, X.; Garay-Reyes, C.G.; Martínez-García, A.; Estrada-Guel, I.; Mendoza-Duarte, J.M.; Guerrero-Seañez, P.; González-Sánchez, S.; Rocha-Rangel, E.; de Jesús Cruz-Rivera, J.; Gutiérrez-Castañeda, E.J.; et al. Enhancement of the Electrical Conductivity and Mechanical Properties of Al-Mg-Si and Al-Mg-Zn Ternary Systems After a T8 Heat Treatment. *Metals* **2024**, *14*, 1286. https://doi.org/10.3390/met14111286

Academic Editor: Joan-Josep Suñol

Received: 25 September 2024
Revised: 6 November 2024
Accepted: 8 November 2024
Published: 13 November 2024



## 1. Introduction

Aluminum (Al) is one of the lightest metals, being, for instance, three times lighter than iron. Aluminum and its alloys possess notable properties, such as high strength and elevated resistance to oxidation, due to the formation of a protective oxide layer on their surface. This characteristic provides exceptional versatility for industrial applications [1]. Additional features that make aluminum and its alloys attractive to the energy sector include their excellent electrical conductivity and compatibility with certain metals [2,3]. For example, pure Al (99.99%) and the 1350 alloy (99.5% min.) exhibit high electrical conductivity, reaching 64.5 and 62%, respectively, according to the International Annealed Copper Standard (IACS) [4,5]. However, both materials have low tensile strength, so alloying Al with other elements is necessary to enhance its mechanical properties, albeit with a slight reduction in electrical conductivity [6].

In recent years, energy consumption has increased significantly, driving the demand for more efficient and durable Al-based electrical conductors [7]. High electrical conductivity is crucial to minimize energy loss during transmission, while substantial mechanical strength is required to endure operational and seasonal mechanical loads [8]. The electrical properties of the alloys used in wire manufacturing are highly sensitive to the type of alloying elements and their microstructure [9]. For instance, electrical resistivity is affected by imperfections in the crystalline structure, which cause electron scattering [10]. These imperfections can include solute atoms, structural defects, and the presence of secondary phases, all of which contribute to changes in the mechanical and electrical properties of the wires [11]. There is a critical need to design and develop new Al-based alloys with superior properties, including increased strength, hardness, and conductivity, over those of commercial alloys. The commercial 6201 and 1350 alloy series are reported to achieve maximum electrical conductivities of 57 and 62% IACS, respectively, which are relatively high, making them suitable for electricity transmission through distribution lines [6]. However, their major limitation lies in their mechanical performance, with maximum tensile strengths of 330 MPa for the 6201 series and 125 MPa for the 1350 series [12,13].

Recently, adding small concentrations of rare earth (RE) metals (such as yttrium, erbium, ytterbium, etc.) to aluminum has become an area of interest, as these additions can achieve an effective combination of strength, ductility, and electrical conductivity [14]. This approach enables the alloy to reach maximum tensile strength values of 240–244 MPa and an electrical conductivity of 57–57.7% IACS. Additionally, with optimal RE addition, electrical conductivity can reach maximum values between 60 and 61.5% IACS; however, the tensile strength decreases to 199–202 MPa, which is relatively low. Although these values surpass those of the 1350 alloy [4,15], Al-REs do not exceed the values observed in 6201 alloys or those found in this study for the fabricated ternary systems.

Conversely, cold plastic deformation is an efficient approach to altering the crystal arrangement, thereby increasing tensile strength and hardness while reducing ductility [16]. Studies have reported increased mechanical strength in alloys used for manufacturing electrical conductors, achieved in laboratory settings through high-deformation processes such as severe plastic deformation (SPD) and rotary swaging (RS) [17]. However, the level of deformation required is too high for practical application in conventional conductive wire manufacturing processes [18,19]. Therefore, it is crucial to study the correlation between mechanical and electrical properties to achieve the optimal balance of strength and electrical conductivity.

According to Fayadomi et al. [20], electron transport is directly proportional to material purity; thus, adding alloying elements generally increases electrical resistivity. However, the resistivity increase is not similar for all elements. For instance, in aluminum alloys, the addition of up to 1 wt. % zinc has been reported to yield higher electrical conductivity than a similar addition of silicon. Additionally, alloying elements are used to enhance strength, corrosion resistance, hardness, and castability [21,22]. Another method for improving the mechanical properties of aluminum alloys is through an aging heat treatment. In age-hardening alloys, the synergistic effect among alloying elements is significant. For example, magnesium and zinc form $Zn_2Mg$, which produces a much higher response to heat treatment than that in the binary Al-Zn system [22]. Likewise, magnesium and silicon favor the formation of $Mg_2Si$ phases, which confer increased strength to these alloys. This approach has been shown to enhance the performance of the 1350 and 6201 alloys, which is expected to have a major impact on the electrical conductor industries. Aluminum alloys typically contain a variety of alloying elements and impurities that contribute to excellent mechanical performance in each alloy. However, these elements can also affect conductivity, which is why it is important to study compositions based on three elements (Al-Mg-Zn and Al-Mg-Si) at low compositions. This research aims to achieve an optimal combination of mechanical properties and electrical conductivity in cold-drawn Al-Mg-Si and Al-Mg-Zn alloy wires by controlling the addition of alloying elements and the T8 temper conditions.

## 2. Materials and Methods

Two ternary alloy systems, Al-Mg-Si and Al-Mg-Zn, were prepared using liquid-state conventional metallurgy methods. The nominal composition of the alloys for this study was determined based on phase diagrams reported in the literature [23,24] (Figure 1). For the Al-Mg-Zn system, two compositions were selected, identified as Al-Mg-Zn-(A) and Al-Mg-Zn-(B). The nominal composition percentages of each alloy are provided in Table 1.

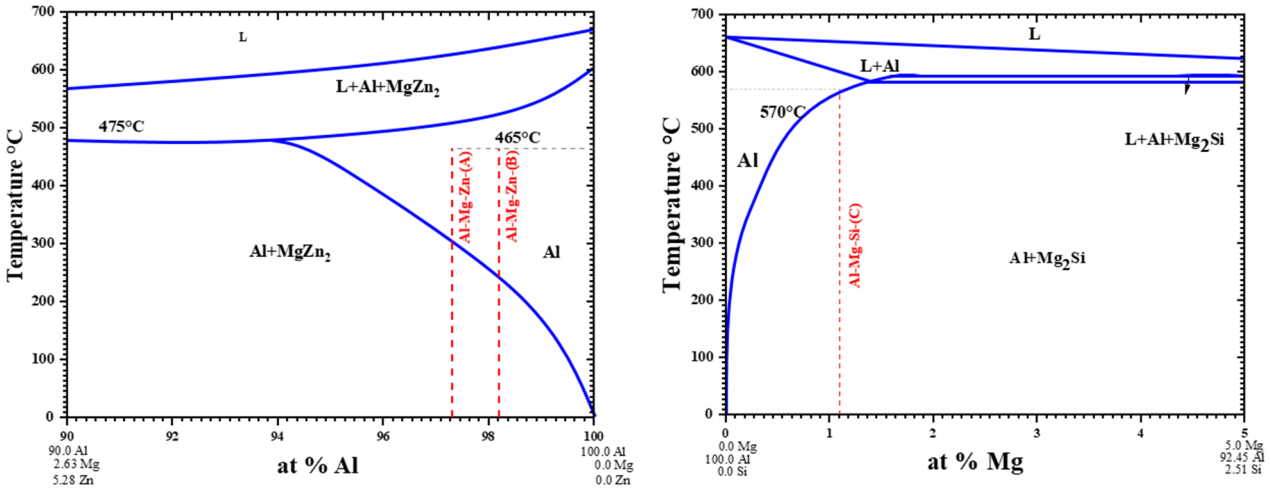


(**a**) (**b**)

**Figure 1.** Phase diagrams of (**a**) Al-$MgZn_2$ and (**b**) Al-$Mg_2Si$ alloys (Adapted from [17,18]). The synthesized compositions are indicated by the dotted red lines.

**Table 1.** Elemental composition of the Al-Mg-Zn-(A), Al-Mg-Zn-(B), and Al-Mg-Si alloy rods utilized in this study. The results were determined through ICP-MS. The composition of commercial alloys 6201 and 1350 is also included.

| Alloys/Elements | Nominal at. % | Experimental ICP at. % | Experimental ICP wt. % | Atomic Ratio | Ref. |
|---|---|---|---|---|---|
| **Al-Mg-Zn–(A)** | | | | **Zn:Mg** | |
| Al | 97.30 | 97.29 | 94.37 | | This work |
| Mg | 0.90 | 0.82 | 0.71 | 2.30 | |
| Zn | 1.80 | 1.89 | 4.46 | | |
| **Al-Mg-Zn–(B)** | | | | **Zn:Mg** | |
| Al | 98.21 | 98.17 | 96.49 | | This work |
| Mg | 0.60 | 0.57 | 0.50 | 2.21 | |
| Zn | 1.20 | 1.26 | 3.00 | | |
| **Al-Mg-Si** | | | | **Mg:Si** | |
| Al | 98.35 | 98.47 | 98.55 | | This work |
| Mg | 1.10 | 1.05 | 0.95 | 2.19 | |
| Si | 0.55 | 0.48 | 0.50 | | |
| **6201** | | | | **Mg:Si** | |
| Al | | | 97.3–98.9 | | [13] |
| Mg | | | 0.60–0.90 | 0.85–1.8 | |
| Si | | | 0.50–0.90 | | |
| **1350** | | | | **Mg:Si** | |
| Al | | | 99.50 | 0.2 | |
| Mg | | | ≤0.05 | **Zn:Mg** | [12] |
| Si | | | ≤0.25 | 1 | |
| Zn | | | ≤0.05 | | |

The melting process was carried out using a LINDBERG BLUE [Riverside, MI, USA] electric furnace set at 740 °C. The process began by melting the aluminum, followed by the addition of the alloying elements Mg-Si and Mg-Zn. Each casting was degassed for 5 min with argon gas using a quartz tube and was manually stirred. After 10 min, the dross was removed from the surface and the molten alloy was poured into cylindrical steel molds to produce cylindrical samples with a height of 100 mm and a diameter of 40 mm.

Cylindrical samples were initially preheated at 450 °C for 30 min and extruded with an extrusion ratio of 16, resulting in rods that were 200 mm long and 10 mm in diameter. Al-Mg-Si and Al-Mg-Zn alloy rods were then subjected to a solution heat treatment (SHT) at 570 and 465 °C for five hours, respectively, using a LINDBERG BLUE electric furnace. Subsequently, the rods were water-quenched to ambient temperature. The temperature for the SHT process was determined based on the eutectic temperature and solvus line (see Figure 1). After SHT, the rods were cold drawn in multiple stages to produce wires with a diameter of approximately 2.54 mm. The wires made of Al-Mg-Si and Al-Mg-Zn alloys were then subjected to aging at temperatures of 200 and 140 °C, respectively. These aging temperatures were chosen based on previous research [16,25,26], to form precipitates of elements such as Mg-Si and Mg-Zn that are in solid solution within the aluminum matrix. Aging times were set at 30, 60, 300, 600, 3000, and 6000 min. Figure 2 illustrates the experimental process sequence utilized in this study to produce the Al-Mg-Si and Al-Mg-Zn alloy wires.

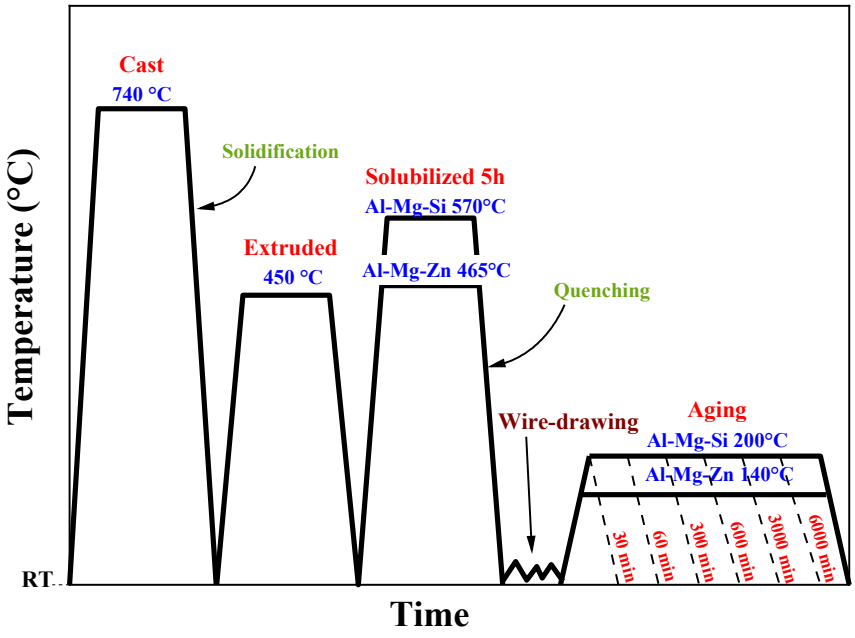


**Figure 2.** Experimental sequence of the deformation processes and thermal treatments utilized in this study.

Samples weighing 2.5 g were taken from Al-Mg-Zn and Al-Mg-Si alloy rods in their as-cast condition for elemental analysis. The chemical composition of the alloys was determined using inductively coupled plasma mass spectrometry (ICP-MS). Tensile and yield strength were measured on six wire specimens that had undergone aging heat treatment, with an approximate diameter of 2.54 mm, using an Instron [Norwood, MA, USA] universal testing machine model 34TM-50, equipped with a 50 kN load cell and a head displacement rate of 10 mm/min. Vickers (HV) microhardness tests were conducted using a 50 g load and 10 s dwell time on an LM300AT LECO [St. Joseph, MI, USA] durometer with ten indentations made on the cross-section of each sample. The minimum spacing between indents was 2.5 times the indent size to comply with the ASTM E92-23 standard [27]. The

structural evolution was assessed using X-ray diffraction (XRD) with a Bruker [Billerica, MA, USA] D8 ADVANCE diffractometer, scanning from 12 to 120° with a step size of 0.016° and a 10 s exposure time. The XRD patterns of the alloys were analyzed using X'Pert HighScore Plus (v2.2b) software, and the samples were prepared metallographically in longitudinal sections. Microstructural characterization was performed using a HITACHI [Chiyoda, TYO, Japan] SU3500 scanning electron microscope, with a working distance of 5.6 mm and a voltage of 10 kV. Micrographs were taken at 200, 500, and 1000 magnifications using a secondary electrons detector and EDS mappings were obtained at 500X for each sample. Samples for this characterization were prepared using conventional metallography techniques and over-etched with Keller reactive to enhance contrast.

Electrical resistivity measurements were conducted four times on wires that were 300 mm long and had cross-sections of 2.54 mm. The electrical conductivity was determined as a percentage of the international Annealed Copper Standard, following the ASTM B193-20 standard and its procedure [28]. Initially, the resistance (the opposition of an object to the flow of electric current, measured in ohms) was determined using Kelvin's method, also known as the "four-point method" [18]. These values were obtained using a Micro Ohm Meter, Keysight (Santa Rosa, CA, USA) model Agilent 34420A.

The resistivity, also known as specific resistance (defined as the resistance per unit length and area of the cross-section of a conductor, measured in ohms m), was calculated using Equation (1).

$$\rho_v = \left(\frac{A}{L}\right) R \tag{1}$$

After obtaining the electrical resistivity, the conductivity ($\sigma$) was calculated (in % IACS) using Equation (2) [28].

$$\sigma = \left(\frac{1}{\rho_v}\right) * 1.7241 \tag{2}$$

where A is the cross-sectional area ($m^2$), L is the length of the wire (m), R is the electrical resistance ($\Omega$), and $\rho_v$ is the electrical resistivity obtained from Equation (1).

## 3. Results

### *3.1. Structural Analysis*

Figure 3 shows the X-ray diffraction patterns of Al-Mg-Zn-(A), Al-Mg-Zn-(B), and Al-Mg-Si alloys in various conditions: as-cast, extruded, wire drawing, and wire drawing aging conditions for 3000 min. The XRD peaks observed in Figure 3a correspond to the aluminum matrix (α-Al), with a face-centered cubic (FCC) structure ($Fm\bar{3}m$) and a lattice parameter of 4.0592 Å in all three alloys. The peaks were identified at 38.37, 44.62, 64.97, 78.10, and 82.31° in 2θ, corresponding to (111), (200), (220), (311), and (222) planes of the α-Al phase. A comparison of the crystalline structure of the as-cast and extruded alloys show a preferential orientation and increased intensity of secondary peaks after extrusion (Figure 3b). Some researchers have reported dynamic recrystallization processes of the Al matrix during high-temperature extrusion of Al alloys [29]. Therefore, it is not surprising that the XRD scan of the aluminum matrix exhibits finer and sharper peaks after extrusion compared to the as-received condition. A higher Mg-Zn content in the alloy results in a preferential orientation along the (200) plane, while a lower Mg-Zn content leads to orientation along the (200) and (220) planes. In contrast, the Al-Mg-Si alloy shows a preferential orientation along the (200) plane (Figure 3b). Changes in grain orientation are influenced by grain boundary migration and the composition of the alloying metals, leading to highly anisotropic grain growth [30]. Consequently, the mechanical and electrical properties of the alloy are dependent on its anisotropy [31]. The cold-drawing process of the rods obtained by extrusion results in noticeable deformation of the crystalline structure in all alloys (Figure 3c), attributed to significant plastic deformation experienced during the drawing process. In Figure 3d, it is evident that the crystallinity of the alloys increases with aging time (3000 min). The orientation of the aged Al-Mg-Zn-(A) and Al-Mg-Si alloys

resembles that of alloys produced by casting, while the orientation of the aged Al-Mg-Zn-(B) alloy is similar to that of alloys produced by extrusion. Due to the detection limit of XRD, secondary phases such as $MgZn_2$ and $Mg_2Si$ were not identified in the alloys obtained by casting, extrusion, wire drawing, and aging (Figure 3a–d).

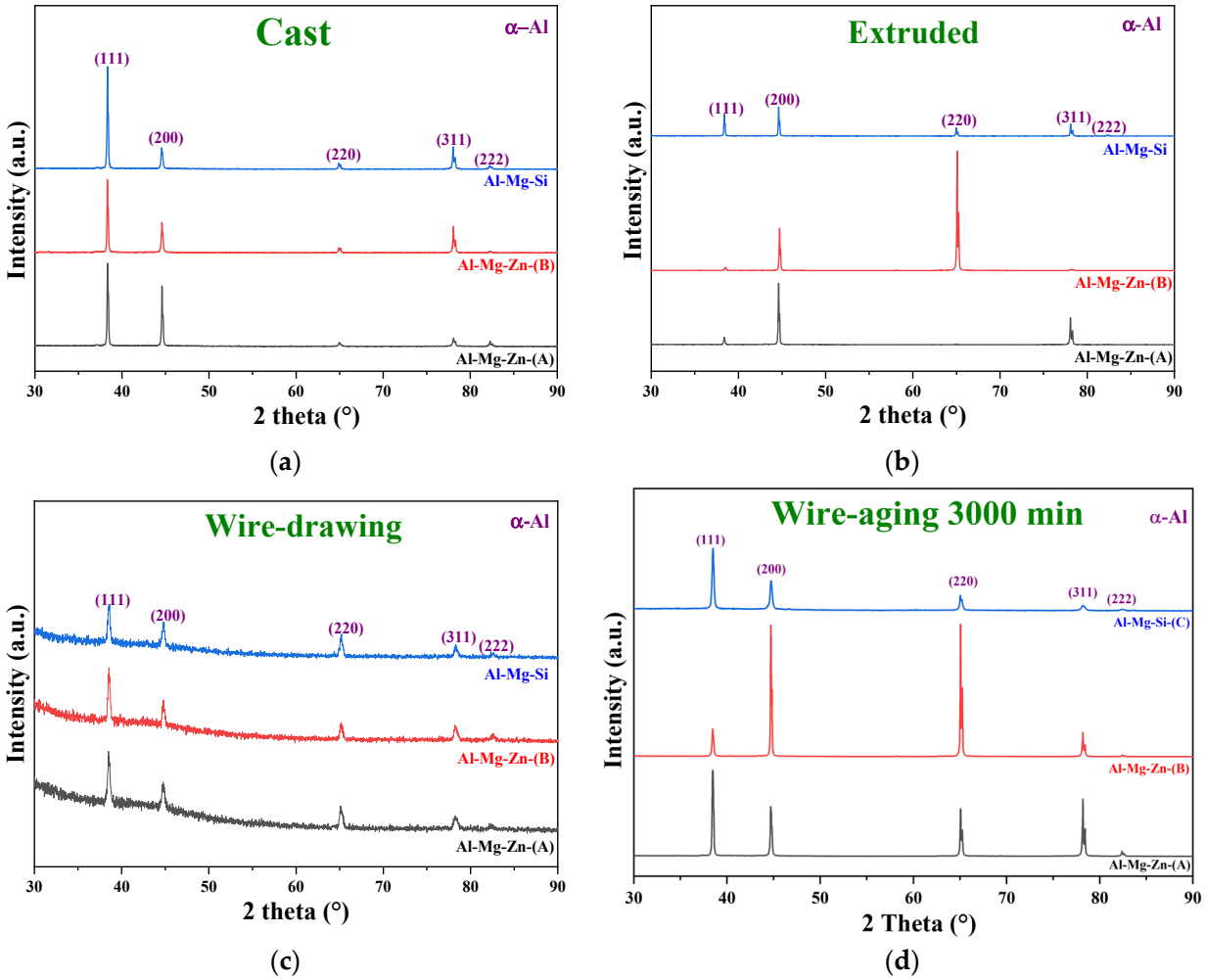


**Figure 3.** X-ray diffraction patterns of Al-Mg-Zn-(A), Al-Mg-Zn-(B), and Al-Mg-Si alloys, after (**a**) casting, (**b**) extrusion, (**c**) wire drawing, and (**d**) wire aging at 3000 min.

On the other hand, the lattice parameter, crystallite size, and cell strain of the alloys were analyzed and are summarized in Table 2. The lattice parameter was determined using Bragg's law for a body-centered cubic lattice (FCC), as shown in Equation (3) [32].

$$d = \left( \frac{a}{\sqrt{h^2 + k^2 + l^2}} \right) \tag{3}$$

where $d$ represents the interplanar distance, $a$ is the lattice parameter, and $h$, $k$, $l$ are the Miller indices. The crystallite size ($D$) and lattice strain ($\varepsilon$) were calculated using the Scherrer equations, as shown in Equations (4) and (5) [33].

$$D = \left( \frac{K\lambda}{\beta cos\theta} \right) \tag{4}$$

$$\varepsilon = \left( \frac{\beta}{4\ tan\theta} \right) \tag{5}$$

**Table 2.** The lattice parameter, crystallite size, and lattice strain were determined using Bragg's law, Scherrer's equations, and the XRD pattern shown in Figure 3.

| Sample | Lattice Parameter (Å) | Crystallite Size (nm) | Strain (ε) |
|---|---|---|---|
| | **Cast** | | |
| Al-Mg-Si | 4.058 ± 0.002 | 35.88 | 0.00183 |
| Al-Mg-Zn-(A) | 4.056 ± 0.002 | 45.61 | 0.00167 |
| Al-Mg-Zn-(B) | 4.058 ± 0.003 | 51.48 | 0.00203 |
| | **Extruded** | | |
| Al-Mg-Si | 4.056 ± 0.001 | 64.24 | 0.00129 |
| Al-Mg-Zn-(A) | 4.057 ± 0.002 | 76.72 | 0.00151 |
| Al-Mg-Zn-(B) | 4.050 ± 0.001 | 58.46 | 0.00207 |
| | **Wire drawn** | | |
| Al-Mg-Si | 4.044 ± 0.003 | 22.83 | 0.00350 |
| Al-Mg-Zn-(A) | 4.046 ± 0.002 | 20.65 | 0.00291 |
| Al-Mg-Zn-(B) | 4.044 ± 0.002 | 27.09 | 0.00316 |
| | **Wire aging 3000 min** | | |
| Al-Mg-Si | 4.049 ± 0.001 | 29.38 | 0.00154 |
| Al-Mg-Zn-(A) | 4.050 ± 0.002 | 55.44 | 0.00127 |
| Al-Mg-Zn-(B) | 4.051 ± 0.002 | 74.47 | 0.00270 |

In this equation, **K** represents a constant with a value of 0.9 for spherical-shaped particles [33], **λ** denotes the wavelength of the copper radiation (1.5406 Å), **θ** represents the diffraction angle for each crystalline plane, and **β** indicates the full-width half maximum (FWHM) of the average height of the reflection in 2θ. Table 2 demonstrates that the binary mixtures of MgZn and MgSi, as well as their concentrations in the alloy, do not impact the lattice parameters of the alloys in solid solution. It is evident that samples processed by casting and extrusion show very similar lattice parameters (**a**-*parameter*) of 4.050 and 4.058 Å, while alloys subjected to wire drawing show a decreased ***a***-*parameter* of 4.044 and 4.046 Å. However, after aging, the ***a***-*parameter* slightly increased to 4.049 and 4.0511 Å, but remained lower than those obtained in the casting and extrusion processes. Samples processed by wire drawing displayed the smallest crystal size and the highest value of lattice strain due to plastic deformation. All samples show positive strain values, indicating the presence of tensile strain exists [34]. Lattice microstrain decreases during the heat treatment of aging primarily due to the annihilation of dislocations by recovery mechanisms below the recrystallization temperature [35]. The alloy with the highest MgZn content (Al-Mg-Zn-(A)) exhibited the lowest lattice strain values, followed by the alloy with MgSi content (Al-Mg-Si), with the highest strain value exhibited by the alloy with the lowest MgZn content (Al-Mg-Zn-(B). However, a higher holding temperature can provide a sufficient driving force for crystallite growth, as observed in the aging wires.

### *3.2. Microstructural and Elemental Analysis*

Figure 4 shows a typical microstructure observed in all alloys following the wire-drawing process. The microstructures of the Al-Mg-Zn-(A), Al-Mg-Zn-(B), and Al-Mg-Si rods are homogeneous, exhibiting a distinct orientation along the extrusion direction.

The sample surface presents elongated grains (with the same elemental composition), as shown in the mappings in Figure 4, in the form of darker zones. Additionally, the presence of pores resulting from the extended etching process is evident. According to the microanalyses and mappings, there is no evidence of the segregation of Mg, Zn, and Si.

Table 1 presents the final composition determined by ICP-MS analysis, which closely matches the initial nominal composition. The atomic ratios of Mg:Si and Zn:Mg for the fabricated systems, as well as for the commercial alloys 6201 and 1350, are provided. Commercial 6201 alloys used for electrical applications typically have Mg:Si atomic ratios below two (ranging from 0.6 to 1.8) [36,37], whereas the alloys in this study have slightly higher Mg:Si and Zn:Mg atomic ratios. The variation in the Mg:Si ratio in commercial

alloys is due to permissible composition ranges, whereas in this study, the Mg:Si ratio was constrained to a value close to two, to maintain the stoichiometry of $Mg_2Si$ precipitates formed during aging heat treatment. In both Al-Mg-Zn alloys, the Zn:Mg ratio was also kept slightly above two, as the hardening phase in this alloy system is $Zn_2Mg$ [38].

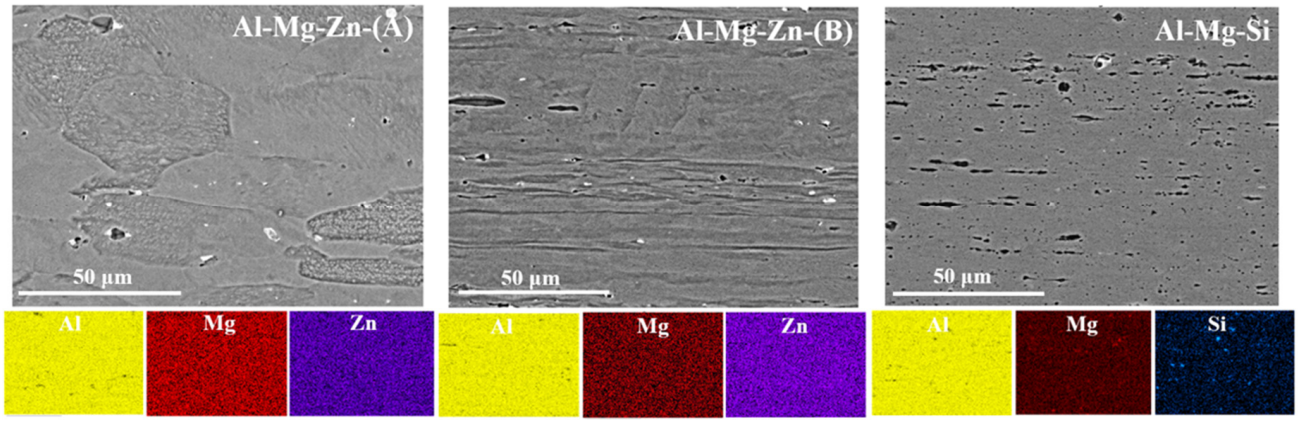


**Figure 4.** SEM micrographs of Al-Mg-Zn-(A), Al-Mg-Zn-(B), and Al-Mg-Si alloy rods after wire drawing along with their corresponding spatial elemental distribution.

### *3.3. Mechanical Response and Electrical Properties*

#### 3.3.1. Tensile Testing

Figure 5 displays the tensile strength ($\sigma_{max}$) values as a function of aging time. The plot includes the $\sigma_{max}$ values from 1350H-16, 6201-T6, and 6201-T8 commercial alloys as reported in the literature [12,13]. This figure indicates that all the obtained values are higher than those for the 1350-H16 and 6201-T6 commercial alloys. Additionally, the sample Al-Mg-Zn-(A) exhibits values greater (350–370 MPa) than 6201-T8 at short aging times (less than 3000 min). Sample Al-Mg-Zn-(B) presents slightly lower values than sample Al-Mg-Si but follows a similar trend. Sample Al-Mg-Zn-(B) demonstrates the highest values (between 286 and 250 MPa), while the Al-Mg-Si sample reaches a maximum between 316 and 301 MPa. Figure 5 also reveals stability in $\sigma_{max}$ values for short aging times and highlights that the reinforcing effect of Zn-Mg is greater than that observed for Mg-Si.

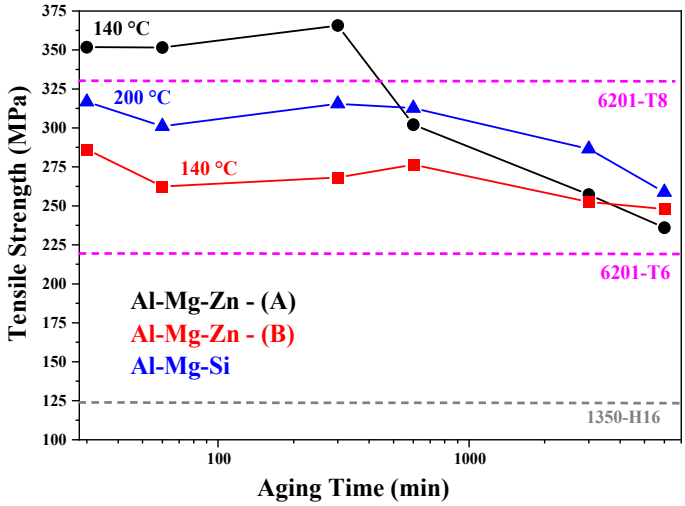


**Figure 5.** Effect of aging time in tensile strength ($\sigma_{max}$) in wire-drawing samples.

The strengthening phases consist of $Mg_2Si$ and $Zn_2Mg$ precipitates [38,39], with characteristics such as number density, spatial distribution, and size, being dependent on the composition, as shown in Figure 5 and Table 1. This table indicates that alloys Al-Mg-Zn-(A)

and Al-Mg-Zn-(B) have a Zn:Mg ratio greater than 2, suggesting that the remaining Zn after precipitation may provide reinforcement by remaining in solid solution in the aluminum matrix. Similarly, in the Al-Mg-Si alloy, the remaining Mg continues to dissolve in the aluminum matrix, and the aging thermal treatment is expected to further enhance reinforcement as indicated by the shorter aging times in Figure 5. According to Reif et al. [40], the mechanism of strength enhancement cannot be solely explained by the addition of various alloying elements and phase transformations. It is also necessary to consider the ability to form stable solid solutions and the feasibility of precipitation hardening.

Zeren [41] investigated the impact of silicon on the tensile strength and elongation percentage in Al-Cu-Si-Mg alloys by adding concentrations ranging from 0 to 18 wt. % silicon. They discovered that increasing silicon content led to an increase in tensile strength, rising from 152 to 200 MPa. However, excessive silicon additions could potentially cause embrittlement in the aluminum alloy [42]. Table 1 in this study demonstrates that the percentage of silicon used in the Si ternary system was 0.50 wt. %, following the experimental procedure outlined in Figure 2. Under these specific conditions, tensile strength values exceeding 300 MPa were achieved, significantly higher than those reported by previous researchers. The 7XXX series aluminum alloys demonstrate high mechanical strength due to the presence of Zn and Mg, leading to the formation of reinforcing $MgZn_2$ precipitates that improve their mechanical properties [43]. As illustrated in Figure 5, sample A, which contains a higher Zn content, exhibits an increase in mechanical strength. Nevertheless, an excessive amount of Zn can have negative consequences starting from the casting. If Zn exceeds 10 wt. %, there is a higher risk of grain coarsening and macro segregation [44,45]. This can lead to an increased likelihood of cracks forming during deformation, ultimately resulting in material fracture [46]. Therefore, it is not advisable to raise the concentration of Zn in the conductor wires analyzed in this study.

#### 3.3.2. Electrical Conductivity and Mechanical Response

Figure 6 shows the electrical conductivity as a function of aging time. This plot includes the % IACS values from the 1350-H16, 6201-T6, and 6201-T8 commercial alloys reported in the literature [12,13]. It can be observed in Figure 6 that alloy (A) shows a lower conductivity concerning the Al-Mg-Zn-(B) and Al-Mg-Si alloys, and the 1350-H16, 6201-T6, and 6201-T8 commercial alloys; nevertheless, conductivity increases from 46 to 52% IACS with longer aging time. The electrical conductivity of the Al-Mg-Zn-(B) alloy is slightly lower than that of the 1350-H16 alloy and higher than those observed in the Al-Mg-Zn-(A), 6201-T6, and 6201-T8 alloys. Due to the insignificant aging effect, greater electrical stability is identified. The Al-Mg-Si alloy reaches a conductivity of 62% IACS, which is very close to that reported for metallic aluminum. This occurs when the alloy is at the maximum aging state (6000 min); at the beginning of the aging heat treatment, the conductivity is below 60% IACS. From Figure 6, it is observed that the Al-Mg-Zn-(B) and Al-Mg-Si alloys have better conductivity values than the commercial alloys commonly used as electrical conductors. From Figure 5, it is observed that the Al-Mg-Si alloy exhibits $\sigma_{max}$ values close to 6201-T8, and the Al-Mg-Zn-(B) alloy shows values slightly lower than Al-Mg-Si. Additionally, both the Al-Mg-Zn-(B) and Al-Mg-Si samples exhibit better $\sigma_{max}$ values than the 6201-T6 alloy. Based on Figures 5 and 6, it is assumed that the Al-Mg-Zn-(B) and Al-Mg-Si alloys present properties ($\sigma_{max}$ and % IACS) that make them competitive against 6201-T8. According to Fadayomi et al. [20], the purity of a material plays a crucial role in enhancing its electrical conductivity. The addition of 0–1 wt. % of solute in aluminum alloys containing transition elements like Zn can maintain conductivity levels higher than those of the silicon that is commonly used as a semiconductor [20,47]. In aged aluminum alloys, the precipitate $MgZn_2$ has a less detrimental impact on conductivity compared to $Mg_2Si$. However, it is essential to determine the optimal composition to achieve improved results with Al-Mg-Zn alloys.

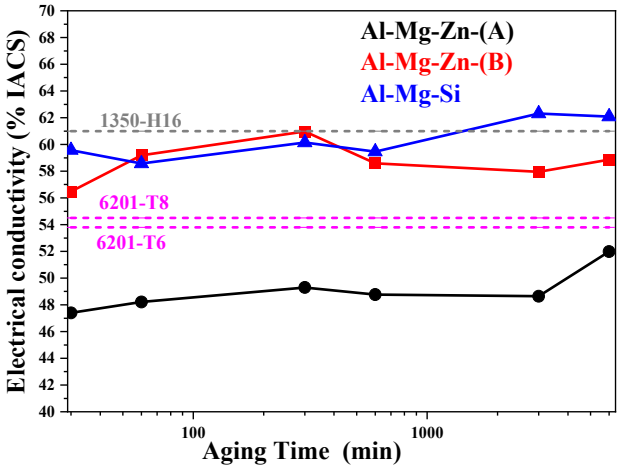


**Figure 6.** Electrical conductivity as a function of the aging time of Al-Mg-Zn–(A), Al-Mg-Zn–(B), and Al-Mg-Si alloy wires.

It has been reported that crystal size and lattice strain influence the electrical properties of materials [48]. XRD analysis revealed that the crystal size and lattice strain (Table 2) of the aged samples for the low-MgZn alloy were 74.47 nm and 0.00270, respectively, while for the Al-Mg-Zn-(A) alloy, values of **D** = 55.44 nm and $\varepsilon$ = 0.00127 were identified. It was observed that the low-MgZn alloy (Al-Mg-Zn-(B)) showed better electrical conductivity properties than the high-MgZn alloy (Al-Mg-Zn-(A)). Studies have indicated that an increase in crystal size has a positive impact on electrical conductivity properties [49]. Therefore, higher values of crystal size and strain could potentially enhance the electrical conductivity properties in this research.

A comparative analysis was conducted on the commercial alloys 6201-T6 and 6201-T8. It was determined that the Al-Mg-Si alloy system presents the strongest correlation between hardness and as shown in Figure 7. The figure shows the electrical conductivity and microhardness values of Al-Mg-Si alloys subjected to cold-drawing (C-D) and aging (1: 30 min, 2: 60 min, 3: 300 min, 4: 600 min, 5: 3000 min and 6: 6000 min) conditions. Moreover, the electrical conductivity and microhardness values of the 1350 and 6201 commercial alloys are provided [12,13]. It is evident that the cold-drawn B alloy and Al-Mg-Si alloys exhibit superior conductivity and hardness compared to the commercial alloys. It is important to note that some values demonstrate higher conductivity than the commercial alloy 1350-H16.

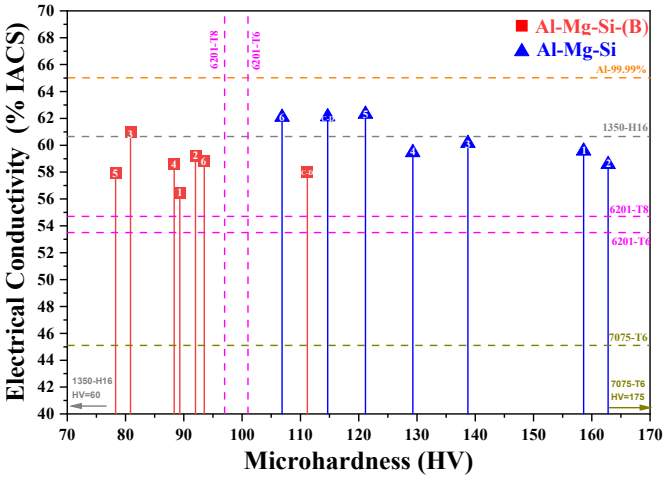


**Figure 7.** Best results found for HV: conductivity to hardness ratio for Al-Mg-Zn-(B) and Al-Mg-Si alloys.

It is well known that an increase in resistance leads to a decrease in electrical conductivity, and conversely, an increase in electrical conductivity results in a decrease in resistance. As shown in Figure 8, the relationship between electrical conductivity and tensile strength is depicted. It is observed that a higher concentration of alloying elements leads to higher mechanical resistance and lower conductivity.

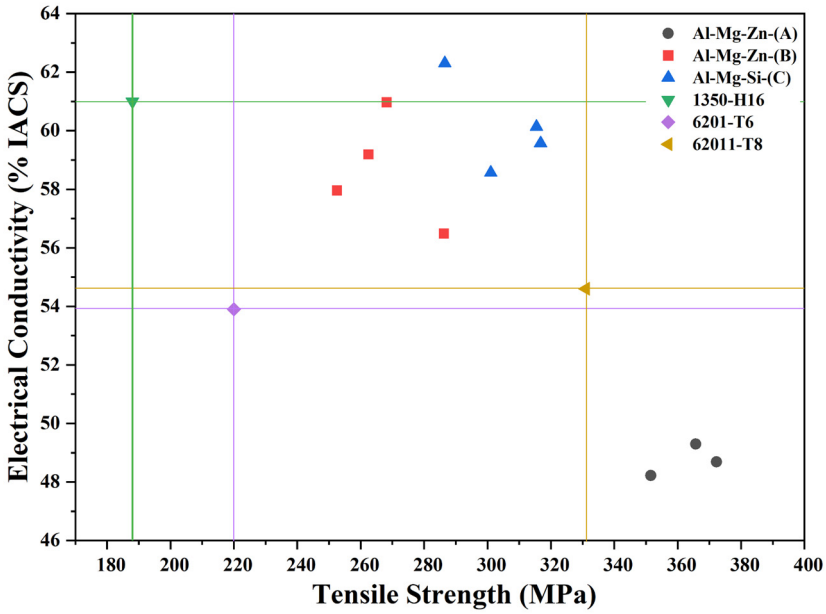


**Figure 8.** Relationship between electrical conductivity and tensile strength.

## 4. Discussion

Cao and Qin [50] evaluated the correlation between conductivity and hardness in an AA7075 alloy. The reported values were 39.8% IACS and 103 HV without heat treatment (NHT). After 5 h of solution treatment, the conductivity increases up to 41.5% IACS, while the hardness decreases to 60 HV. Similarly, mechanical behavior and electrical conductivity properties comparable to those of the 6201-T6 alloy have been reported in sheets of an Al-0.2Fe-0.06Cu alloy modified with 0.1 and 0.15 wt. % La [51]. Despite the favorable strength-to-electrical conductivity ratio, lanthanum has not been widely used as an alloying element due to its high density, toxicity, and need for careful handling. Furthermore, there have been no reported evaluations of samples synthesized through a standard wire manufacturing process (wire drawing).

There are exceptional cases where the mechanical response of a conductive alloy can be enhanced without significantly impacting the electrical conductivity [18]. These cases employ controlled, high-deformation processes in the laboratory, such as high-pressure torsion and rotary swaging (RS).

According to Mao et al., the best combinations of electrical conductivity and maximum tensile strength are 50.6% IACS and 363 MPa, and 51.7% IACS and 352 MPa, achieved through under-aging (550 °C/3 h + 175 °C/2 h) + RS + re-aging (160 °C/4 h) and peak aging (550 °C/3 h + 175 °C/8 h) + RS + re-aging (160 °C/4 h) for samples containing Al-Mg-Si [19]. This highlights that the processing route significantly influences electrical conductivity. The reduced electrical conductivity of Al alloys is due to the negative effect of alloying elements on electron mobility, unlike in pure aluminum where this effect is absent. During aging, alloying elements are released from the supersaturated aluminum matrix, enhancing conductivity. Figure 9 shows the tensile strengths of Al-Mg-Zn-(A), Al-Mg-Zn-(B), and Al-Mg-Si alloys at various aging times (30, 60, and 300 min) for alloys processed by a conventional wire manufacturing route, compared to values reported in the literature for wires in T6 and T8 conditions. Unlike an ultrafine microstructure achieved through highly controlled, high-deformation processes, this figure demonstrates that alloying elements

and composition are key to achieving the desired mechanical properties in alloys intended for similar applications.

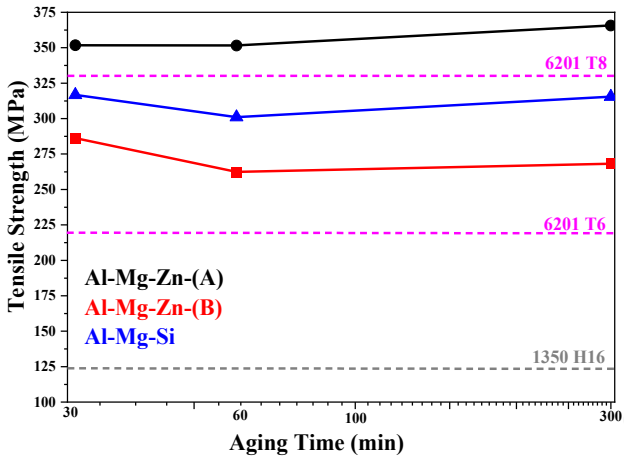


**Figure 9.** Tensile strength as a function of the aging time; section was extracted from Figure 5.

The high zinc content in the Al-Mg-Zn-(A) alloy enhances precipitation hardening during thermal aging treatment, resulting in higher values compared to those reported for the commercial 6201-T8 alloy. In the case of Al-Mg-Zn-(B), the values are very similar to those observed for the commercial alloy. The Al-Mg-Si alloy shows lower values than the Al-Mg-Zn-(B) alloy, although its values still surpass those of 6201-T6 and 1350-H16. It is important to note that none of the three alloys have reached the overaged condition, suggesting that an even better mechanical response may be achievable. Figure 10 presents conductivity values as a function of short aging times. From this figure, it can be observed that high alloying element concentrations (Al-Mg-Zn-(A) alloy) do not promote electrical conductivity. However, the Al-Mg-Zn-(B) and Al-Mg-Si alloys, with lower alloying element contents (Table 1), display higher conductivity values at short aging times. This emphasized the importance of the type of precipitates formed during aging. In the Al-Mg-Zn-(B) alloy, $MgZn_2$ precipitates are formed, whereas in the Al-Mg-Si alloy, the precipitates are $Mg_2Si$ (metal–metalloid). Conductivity increases with aging time due to partial purification of the aluminum matrix as alloying elements are expelled during aging to form precipitates. Impurities, alloying elements, second phases, and precipitates act as scatterers of electron pathways in conductive materials, which explains the superior conductivity of the Al-Mg-Si alloy at longer aging times.

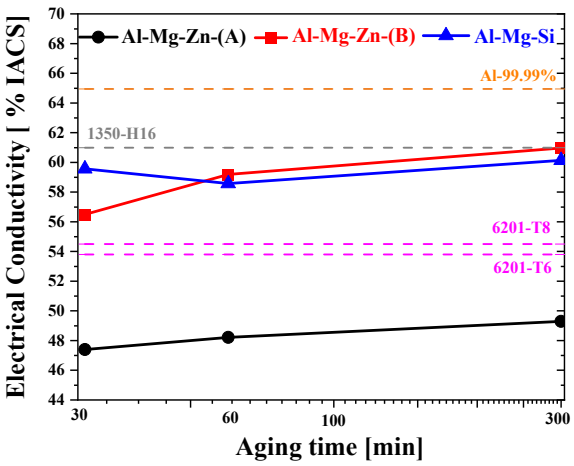


**Figure 10.** Electrical conductivity versus aging time; section taken from Figure 6.

Dean [52] discusses the impact of alloying elements and impurities on the electrical conductivity of aluminum alloys. Based on this reference, Table 3 presents the contributions of Mg, Si, and Zn in reducing conductivity. This table summarizes the maximum solubility of various elements in aluminum, along with the average increase in resistivity per 1.0 wt. % of each element, both in solution and out of solution. The effect of each element can be calculated as shown in the following example for the Al-Mg-Zn-(A) ternary system: if the alloy contains 4.46 wt. % Zn and 0.71 wt. % Mg and both are out of solution, the increase in resistivity of high-purity aluminum (2.65 μΩ cm at 20 °C) would be calculated as follows:

$$0.023 \times 4.46 + 0.22 \times 0.71 = 0.25878\ \mu\Omega\ \text{cm}$$

**Table 3.** Effect of elements in and out of solid solution on the resistivity of aluminum (Adapted from [52]). The background color refers to the elements used in this research.

| Element | Maximum Solubility in Aluminum % | Average Increase in Resistivity per wt. % μΩ·cm | |
|---|---|---|---|
| | | In Solution | Out Solution |
| Chrome | 0.77 | 4.00 | 0.180 |
| Copper | 5.65 | 0.34 | 0.30 |
| Iron | 0.05 | 2.56 | 0.058 |
| Lithium | 4.00 | 3.31 | 0.680 |
| Magnesium | 14.90 | 0.54 | 0.220 |
| Manganese | 1.82 | 2.94 | 0.349 |
| Nickel | 0.05 | 0.81 | 0.061 |
| Silicon | 1.65 | 1.02 | 0.088 |
| Titanium | 1.00 | 2.88 | 0.120 |
| Vanadium | 0.50 | 3.58 | 0.280 |
| Zinc | 82.8 | 0.09 | 0.023 |
| Zirconium | 0.28 | 1.74 | 0.044 |

Considering the data presented in Table 1 and the impact of elements on aluminum resistivity as shown in Table 3, the most conductive alloy is expected to be the Al-Mg-Zn-(B) alloy, followed by the Al-Mg-Zn-(A) alloy, and, finally, the Al-Mg-Si alloy. These findings are consistent with experimental results for the two Al-Mg-Zn alloys, which have distinct compositions, and demonstrate the significant effects of Mg and Zn. Experimental data show that the Al-Mg-Si alloy is one of the most conductive alloys, despite theoretical calculations suggesting it to be the least conductive.

This analysis highlights the importance of controlling alloy composition, determining the appropriate solution heat treatment for each composition (temperature and time), and establishing the optimal aging temperature for each composition to obtain a more representative aging curve. For Zn alloys, it is important to assess if the T8 treatment is the most suitable.

## 5. Conclusions

This study focuses on improving the mechanical properties and electrical conductivity of two ternary alloys, Al-Mg-Zn and Al-Mg-Si, prepared using standard conductive wire manufacturing techniques complemented by T8 tempering (solution heat treated, cold worked, and artificially aged). Experimental results were compared to commercial 6201-T8 and 1350-H16 alloys. Compositional and processing parameters were adjusted to achieve the optimal balance of electrical conductivity and high strength. The inclusion of Zn-Mg and Mg-Si as alloying elements in the aluminum matrix promotes the formation of precipitates during aging heat treatment, enhancing mechanical properties while maintaining electrical resistivity at levels that make these alloys excellent electrical conductors. Sample wires with high electrical conductivity were fabricated from Al-Mg-Si and Al-Mg-Zn-(B) compositions, achieving conductivity values of 62% and 61% IACS, respectively. These alloys are strong

candidates against commercial 6201 and 1350-H16 alloys. While both systems exhibit similar conductivities, they demonstrate superior mechanical properties compared to the 1350-H16 alloy, with enhanced tensile strengths of up to 275 MPa. The study suggests that further optimization of solution treatment and aging conditions will be necessary to maximize the mechanical and electrical performance of the investigated alloys.

**Author Contributions:** Conceptualization, X.A.-S., C.G.G.-R. and R.M.-S.; methodology, X.A.-S., C.G.G.-R., E.R.-R. and R.M.-S.; software, J.M.M.-D. and P.G.-S.; validation, E.R.-R., E.J.G.-C. and S.G.-S.; formal analysis, J.d.J.C.-R., S.G.-S. and R.M.-S.; investigation, Atanacio-Sánchez, C.G.G.-R., A.M.-G., P.G.-S., E.R.-R., I.E.-G. and R.M.-S.; resources, I.E.-G. and R.M.-S.; data curation, Atanacio-Sánchez, C.G.G.-R., A.M.-G., J.M.M.-D., P.G.-S., S.G.-S., J.d.J.C.-R., E.J.G.-C., I.E.-G. and R.M.-S.; writing—original draft, X.A.-S., C.G.G.-R., A.M.-G. and R.M.-S.; writing—review and editing, X.A.-S., C.G.G.-R., A.M.-G., I.E.-G., P.G.-S., E.R.-R., J.d.J.C.-R., E.J.G.-C. and R.M.-S.; visualization, J.M.M.-D. and S.G.-S.; supervision, C.G.G.-R., I.E.-G. and R.M.-S. All authors have read and agreed to the published version of the manuscript.

**Funding:** This research received no external funding.

**Data Availability Statement:** The original contributions presented in the study are included in the article, further inquiries can be directed to the corresponding author.

**Acknowledgments:** The authors thank A. I. Gonzalez-Jacquez, K. Campos-Venegas, F. Nevarez-Vargas, and R. Bernal-Gonzalez for their valuable technical support throughout the study. The Research Center in Advanced Materials (CIMAV) supported this work.

**Conflicts of Interest:** The authors declare that they have no interests or personal relationships that could influence the work reported in this paper.

## References

1. Gandara, M.J.F. Aluminium: The metal of choice. *Mater. Technol.* **2013**, *47*, 261–265.
2. Dokšanović, T.; Džeba, I.; Markulak, D. Variability of structural aluminium alloys mechanical properties. *Struct. Saf.* **2017**, *67*, 11–26. [CrossRef]
3. Varshney, D.; Kumar, K. Application and use of different aluminium alloys with respect to workability, strength and welding parameter optimization. *Ain Shams Eng. J.* **2021**, *12*, 1143–1152. [CrossRef]
4. Liu, L.; Jiang, J.-T.; Zhang, B.; Shao, W.-Z.; Zhen, L. Enhancement of strength and electrical conductivity for a dilute Al-Sc-Zr alloy via heat treatments and cold drawing. *J. Mater. Sci. Technol.* **2019**, *35*, 962–971. [CrossRef]
5. Kaufman, J.G. Properties of Pure Aluminum. In *Aluminum Science and Technology*; Anderson, K., Weritz, J., Kaufman, J.G., Eds.; ASM International: Almere, The Netherlands, 2018.
6. *European Standard EN 50183*; Conductors of Aluminium Alloy with Magnesium and Silicon Content. European Committee for Standardization: Brussels, Belgium, 2002.
7. Rocha, P.; Langlois, S.; Lalonde, S.; Araújo, J.; Castro, F. Influence of 1350 and 6201 aluminum alloys on the fatigue life of overhead conductors—A finite element analysis. *Tribol. Int.* **2023**, *186*, 108661. [CrossRef]
8. Cui, X.; Wu, Y.; Liu, X.; Zhao, Q.; Zhang, G. Effects of grain refinement and boron treatment on electrical conductivity and mechanical properties of AA1070 aluminum. *Mater. Des.* **2015**, *86*, 397–403. [CrossRef]
9. Abdo, H.S.; Seikh, A.H.; Mohammed, J.A.; Soliman, M.S. Alloying Elements Effects on Electrical Conductivity and Mechanical Properties of Newly Fabricated Al Based Alloys Produced by Conventional Casting Process. *Materials* **2021**, *14*, 3971. [CrossRef]
10. Rossiter, P.L. *The Electrical Resistivity of Metals and Alloys*; Cambridge University Press: Cambridge, UK, 1991; Volume 6.
11. Guan, R.; Shen, Y.; Zhao, Z.; Wang, X. A high-strength, ductile Al-0.35 Sc-0.2 Zr alloy with good electrical conductivity strengthened by coherent nanosized-precipitates. *J. Mater. Sci. Technol.* **2017**, *33*, 215–223. [CrossRef]
12. *Aluminum 1350-H16*; Aluminum Standards and Data 2000. Matweb: Blacksburg, VA, USA, 2024.
13. *Aluminum 6201-T6*; Aluminum Standards and Data 2000. Matweb: Blacksburg, VA, USA, 2024.
14. Harada, Y.; Dunand, D. Microstructure of Al3Sc with ternary transition-metal additions. *Mater. Sci. Eng. A* **2002**, *329*, 686–695. [CrossRef]
15. Gorlov, L.; Loginova, I.; Glavatskikh, M.; Barkov, R.; Pozdniakov, A. Novel precipitation strengthened Al-Y-Sc-Er alloy with high mechanical properties, ductility and electrical conductivity produced by different thermomechanical treatments. *J. Alloys Compd.* **2022**, *918*, 165748. [CrossRef]
16. Karabay, S. Influence of AlB2 compound on elimination of incoherent precipitation in artificial aging of wires drawn from redraw rod extruded from billets cast of alloy AA-6101 by vertical direct chill casting. *Mater. Des.* **2008**, *29*, 1364–1375. [CrossRef]
17. Lim, S.J.; Choi, H.J.; Na, K.H.; Lee, C.H. Dimensional characteristics of products using rotary swaging machine with four-dies. *Solid State Phenom.* **2007**, *124*, 1645–1648. [CrossRef]

18. Valiev, R.Z.; Murashkin, M.Y.; Sabirov, I. A nanostructural design to produce high-strength Al alloys with enhanced electrical conductivity. *Scr. Mater.* **2014**, *76*, 13–16. [CrossRef]
19. Mao, Q.; Wang, L.; Nie, J.; Zhao, Y. Optimizing strength and electrical conductivity of 6201 aluminum alloy wire through rotary swaging and aging processes. *J. Mater. Process. Technol.* **2024**, *331*, 118497. [CrossRef]
20. Fadayomi, O.; Clark, R.; Thole, V.; Sanders, P.G.; Odegard, G.M. Investigation of Al-Zn-Zr and Al-Zn-Ni alloys for high electrical conductivity and strength application. *Mater. Sci. Eng. A* **2019**, *743*, 785–797. [CrossRef]
21. Dobrzański, L.A.; Totten, G.E.; Bamberger, M. The importance of magnesium and its alloys in modern technology and methods of shaping their structure and properties. In *Magnesium and Its Alloys*; CRC Press: Boca Raton, FL, USA, 2019; pp. 1–28.
22. Prasad, S.V.S.; Verma, K.; Mishra, R.K.; Kumar, V.; Singh, S. The role and significance of Magnesium in modern day research-A review. *J. Magnes. Alloys* **2022**, *10*, 1–61. [CrossRef]
23. Okamoto, H.; Villars, P. (Eds.) *Al-Mg-Zn Vertical Section of Ternary Phase*; Material Phases Data System (MPDS); Springer: Berlin/Heidelberg, Germany, 2022.
24. Hari Kumar, K.C.; Chakraborti, N.; Lukas, H.L.; Bodak, O.; Rokhlin, L.; Materials Science International Team MSIT®. *Section from Al to $Mg_2Si$: Datasheet from MSI Eureka in Springer Materials*; Effenberg, G., Ed.; MSI, Materials Science International Services GmbH: Stuttgart, Germany, 2004. Available online: https://materials.springer.com/msi/phase-diagram/docs/sm_msi_r_10_014594_03_full_LnkDia0 (accessed on 15 October 2023).
25. Allamki, A.; Al-Maharbi, M.; Arunachalam, R.; Qamar, S.Z. Improved tensile strength and electrical conductivity of the electrical conductor aluminum alloy 6201. In *ASME International Mechanical Engineering Congress and Exposition*; American Society of Mechanical Engineers: New York, NY, USA, 2021.
26. Kim, Y.-W.; Jo, Y.-H.; Lee, Y.-S.; Kim, H.-W.; Lee, J.-I. Effect of Dissolution of η′ Precipitates on Mechanical Properties of A7075-T6 Alloy. *Korean J. Met. Mater.* **2022**, *60*, 83–93. [CrossRef]
27. *ASTM E92-23*; Standard Test Methods for Vickers Hardness and Knoop Hardness of Metallic Materials. ASTM International: West Conshohocken, PA, USA, 2023.
28. *ASTM B193-20*; Standard Test Method for Resistivity of Electrical Conductor Materials. ASTM: West Conshohocken, PA, USA, 2023.
29. Yang, B.; Gao, M.; Wang, Y.; Guan, R. Dynamic recrystallization behavior and mechanical properties response of rheo-extruded Al–Mg alloys with various Mg contents. *Mater. Sci. Eng. A* **2022**, *849*, 143450. [CrossRef]
30. Humphreys, F.J.; Hatherly, M. *Recrystallization and Related Annealing Phenomena*; Elsevier: Amsterdam, The Netherlands, 2012.
31. Frodal, B.H.; Thomesen, S.; Børvik, T.; Hopperstad, O.S. On fracture anisotropy in textured aluminium alloys. *Int. J. Solids Struct.* **2022**, *244*, 111563. [CrossRef]
32. Bragg, W.H.; Bragg, W.L. The reflection of X-rays by crystals. *Proc. R. Soc. Lond. Ser. A Contain. Pap. A Math. Phys. Character* **1913**, *88*, 428–438. [CrossRef]
33. Scherrer, P. Bestimmung der Grosse und inneren Struktur von Kolloidteilchen mittels Rontgenstrahlen. *Nach Ges Wiss Gottingen* **1918**, *2*, 8–100.
34. Ahlawat, A.; Sathe, V.; Reddy, V.; Gupta, A. Mossbauer, Raman and X-ray diffraction studies of superparamagnetic $NiFe_2O_4$ nanoparticles prepared by sol–gel auto-combustion method. *J. Magn. Magn. Mater.* **2011**, *323*, 2049–2054. [CrossRef]
35. Zhao, F.; Xu, X.; Liu, H.; Wang, Y. Effect of annealing treatment on the microstructure and mechanical properties of ultrafine-grained aluminum. *Mater. Des.* **2014**, *53*, 262–268. [CrossRef]
36. *ASTM B398/B398M-22*; Standard Specification for Aluminum-Alloy 6201-T81 and 6201-T83 Wire for Electrical Purposes. ASTM: West Conshohocken, PA, USA, 2023.
37. Dong, Q.; Zhang, Y.; Wang, J.; Huang, L.; Nagaumi, H. Enhanced strength-conductivity trade-off in Al-Mg-Si alloys with optimized Mg/Si ratio. *J. Alloys Compd.* **2024**, *970*, 172682. [CrossRef]
38. Stiller, K.; Warren, P.J.; Hansen, V.; Angenete, J.; Gjønnes, J. Investigation of precipitation in an Al–Zn–Mg alloy after two-step ageing treatment at 100 and 150 C. *Mater. Sci. Eng. A* **1999**, *270*, 55–63. [CrossRef]
39. Kumar, K.A.; Pillai UT, S.; Pai, B.C.; Chakraborty, M. Dry sliding wear behaviour of Mg–Si alloys. *Wear* **2013**, *303*, 56–64. [CrossRef]
40. Reif, W.; Dutkiewicz, J.; Ciach, R.; Yu, S.; Król, J. Effect of ageing on the evolution of precipitates in AlSiCuMg alloys. *Mater. Sci. Eng. A* **1997**, *234*, 165–168. [CrossRef]
41. Zeren, M. Effect of copper and silicon content on mechanical properties in Al–Cu–Si–Mg alloys. *J. Mater. Process. Technol.* **2005**, *169*, 292–298. [CrossRef]
42. Otani, Y.; Sasaki, S. Effects of the addition of silicon to 7075 aluminum alloy on microstructure, mechanical properties, and selective laser melting processability. *Mater. Sci. Eng. A* **2020**, *777*, 139079. [CrossRef]
43. Qi, T.; Zhu, H.; Zhang, H.; Yin, J.; Ke, L.; Zeng, X. Selective laser melting of Al7050 powder: Melting mode transition and comparison of the characteristics between the keyhole and conduction mode. *Mater. Des.* **2017**, *135*, 257–266. [CrossRef]
44. Shin, S.-S.; Won, S.-J.; So, H.; Lee, S.-K.; Kim, K.-H. High-strength Al-Zn-Cu-based alloy synthesized by high-pressure die-casting method. *Metall. Mater. Trans. A* **2020**, *51*, 6630–6639. [CrossRef]
45. Oñoro, J. The stress corrosion cracking behaviour of heat-treated Al–Zn–Mg–Cu alloy in modified salt spray fog testing. *Mater. Corros.* **2010**, *61*, 125–129. [CrossRef]

46. Jiang, H.; Xing, H.; Xu, Z.; Yang, B.; Liang, E.; Zhang, J.; Sun, B. Effect of Zn content and Sc, Zr addition on microstructure and mechanical properties of Al-Zn-Mg-Cu alloys. *J. Alloys Compd.* **2023**, *947*, 169246. [CrossRef]
47. Heywang, W.; Zaininger, K. Silicon: The semiconductor material. In *Silicon: Evolution and Future of a Technology*; Springer: Berlin/Heidelberg, Germany, 2004; pp. 25–42.
48. Abbas, S.F.; Kim, T.-S. Effect of lattice strain on the electrical conductivity of rapidly solidified copper-iron metastable alloys. *J. Alloys Compd.* **2018**, *732*, 129–135. [CrossRef]
49. Raja, G.; Nallathambi, A.; Prakasam, A.; Gopinath, S.; Ragupathi, C.; Narayanan, S.; Tamizhdurai, P.; Kumaran, R.; Alsaiari, N.S.; Abualnaja, K.M.; et al. Effect of lattice strain on structure, morphology, electrical conductivity and magneto-optical and catalytic properties of Ni-doped Mn3O4 nano-crystallites synthesized by microwave route. *J. Saudi Chem. Soc.* **2022**, *26*, 101440. [CrossRef]
50. Cao, F.; Qin, Z. Effect of two-stage aging on hardness and electrical conductivity of as-extruded 7075 aAluminum Alloy. *J. Phys. Conf. Ser.* **2021**, *1885*, 042035. [CrossRef]
51. Lu, L.; Shen, Y.; Chen, X.; Qian, L.; Lu, K. Ultrahigh strength and high electrical conductivity in copper. *Science* **2004**, *304*, 422–426. [CrossRef]
52. Dean, W.A. *Properties and Physical Metallurgy*; ASM International: Materials Park, OH, USA, 1984; Chapter 6; pp. 200–241.